





34

35

### Abstract

36 In the summer of 2017, heavy ozone pollution swamped most of the North China Plain (NCP),  
37 with the maximum regional average of daily maximum 8-h ozone concentration (MDA8) reaching  
38 almost 120 ppbv. In light of the continuing reduction of anthropogenic emissions in China, the  
39 underlying mechanisms for the occurrences of these regional extreme ozone episodes are  
40 elucidated from two perspectives: meteorology and biogenic emissions. The significant positive  
41 correlation between MDA8 and temperature, which is amplified during heat waves concomitant  
42 with stagnant air and no precipitation, supports the crucial role of meteorology in driving high  
43 ozone concentrations. We also find that biogenic emissions are enhanced due to factors previously  
44 not considered. During the heavy ozone pollution episodes in June 2017, biogenic emissions driven  
45 by high vapor pressure deficit (VPD), land cover change and urban landscape yield an extra mean  
46 MDA8 ozone of 3.08, 2.79 and 4.74 ppbv, respectively over the NCP, which together contribute  
47 as much to MDA8 ozone as biogenic emissions simulated using the land cover of 2003 and  
48 ignoring VPD and urban landscape. In Beijing, the biogenic emission increase due to urban  
49 landscape has a comparable effect on MDA8 ozone to the combined effect of high VPD and land  
50 cover change between 2003 and 2016. This study highlights the vital contributions of heat waves,  
51 land cover change and urbanization to the occurrence of extreme ozone episode, with significant  
52 implications for ozone pollution control in a future when heat wave frequency and intensity are  
53 projected to increase under global warming.

54

### Keywords

56 Ozone pollution, heat waves, biogenic emission, land cover change, urban landscape

57



## 58 1 Introduction

59 In recent decades, China has been facing severe air pollution issues, particularly for the winter  
60 PM<sub>2.5</sub> and summer ozone (Zheng et al., 2015; Cheng et al., 2016; Zhao et al., 2016). It has been  
61 noted that the mean concentration of PM<sub>2.5</sub> has generally decreased in the past few years but the  
62 concentration of O<sub>3</sub> shows an increasing trend (Li et al., 2017b; Wang et al., 2017; Chen et al.,  
63 2018a; Li et al., 2019), suggesting a greater urgency for ozone pollution control. For instance, Li  
64 et al. (2017b) revealed an increase of annual mean ozone in 2016 by 11 μg/m<sup>3</sup> compared to 2014  
65 in China. Lu et al. (2018) found a 3.7-6.2% increase per year in the mean ozone concentration  
66 over 74 cities in China from 2013 to 2017. Since ozone is harmful to both human health (Soriano  
67 et al., 2017) and vegetation (Emberson et al., 2009; Avnery et al., 2011), it is vital to investigate  
68 the possible mechanisms related to high ozone concentrations. Based on ozone observations  
69 from 2013-2017, the North China Plain (NCP, an area about 400,000 km<sup>2</sup> in size with Beijing  
70 located on its northeast edge), is identified as the area with the most severe ozone pollution in  
71 China compared to other regions such as the Yangtze River Delta and Pearl River Delta, possibly  
72 linked to the stimulation effect from enhanced hydroperoxy radicals (HO<sub>2</sub>) due to reduction in  
73 aerosol sink resulting from the decrease of PM<sub>2.5</sub> during this period (Li et al., 2019). Chen et al.  
74 (2019) investigated the impact of meteorological factors such as temperature, wind speed and  
75 solar radiation on ozone pollution from 2006-2016 and noted that the severe ozone events in  
76 June 2017 around Beijing stand out and suggested a possible connection with the abnormal  
77 meteorological conditions. These studies motivated a need for a better understanding of the high  
78 ozone problem over NCP.

79 Tropospheric ozone is closely related to both anthropogenic emissions and biogenic  
80 emissions, including volatile organic compounds (VOCs) and nitrogen oxides (NO<sub>x</sub>) (Sillman,  
81 1995, 1999; Tonnesen and Dennis, 2000; Xing et al., 2011; Fu et al., 2012). In the past few years  
82 (i.e., 2012-2017), anthropogenic emissions such as NO<sub>x</sub> continued to decrease (Liu et al., 2016)  
83 and anthropogenic VOCs changed little (Zhao et al., 2018; Zheng et al., 2018; Li et al., 2019).  
84 Biogenic VOCs (BVOC) were reported to enhance hourly ozone by 3-5 ppbv in NCP, especially  
85 in areas north of Beijing, based on a two-day simulation from July 31 to August 1, 1999 (Wang  
86 et al., 2008). The annual BVOC emission in this area increased by 1-1.5% per year from 1979-  
87 2012 (Stavrakou et al., 2014) due to changes of land use and climate. Broadleaf trees in general



88 have a higher emission rate of BVOC than grass, shrub and crops (Guenther et al., 2012). A  
89 dramatic increase of forest (trees) coverage is evident in the last 20 years over NCP (Chen et al.,  
90 2018b), partly attributable to the “Three-north Forest Protection Project”. For example, trees  
91 planted before the 2008 Olympic Games doubled the BVOC emissions in Beijing from 2005 to  
92 2010 (Ghirardo et al., 2016). Urban landscape may even emit more BVOC than natural forest  
93 because of favorable conditions such as lower tree densities and better light illumination (Ren et  
94 al., 2017). Ren et al. (2017) found that BVOC emitted by urban landscape accounted for 15% of  
95 total BVOC emissions in Beijing in 2015. Over highly polluted urban areas of the NCP, ozone  
96 production is highly sensitive to VOC emissions (Liu et al., 2012; Han et al., 2018). Therefore,  
97 elevated BVOC emissions can greatly enhance ozone formation in NCP.

98 Besides emissions, tropospheric ozone is also closely related to meteorological conditions,  
99 such as heat waves (Gao et al., 2013; Fiore et al., 2015; Otero et al., 2016), low wind speed and  
100 stagnant weather (Jacob and Winner, 2009; Sun et al., 2017; Zhang et al., 2018). Weather  
101 conditions concomitant with heat waves including high temperature, low wind speed, and little  
102 cloud coverage may enhance ozone production (Jaffe and Zhang, 2017; Pu et al., 2017; Sun et  
103 al., 2019). At the same time, such meteorological conditions also promote emissions of BVOC  
104 and ozone formation (Zhang and Wang, 2016). Using a global model, Fu and Liao (2014)  
105 suggested a slight-to-moderate increase of biogenic isoprene west and north of Beijing due to  
106 land cover and land use alone, and an even more obvious increase when meteorological changes  
107 are considered. In the summer of 2017, heat waves swept over a majority of area of NCP,  
108 providing an excellent opportunity to investigate how the heat wave may have modulated  
109 biogenic VOC emissions and subsequent severe ozone events in NCP. Observation data and  
110 modeling are used to delineate various factors contributing to enhanced biogenic emissions and  
111 elevated ozone concentrations. More details of the data and model are provided in Methods.

112

113

114

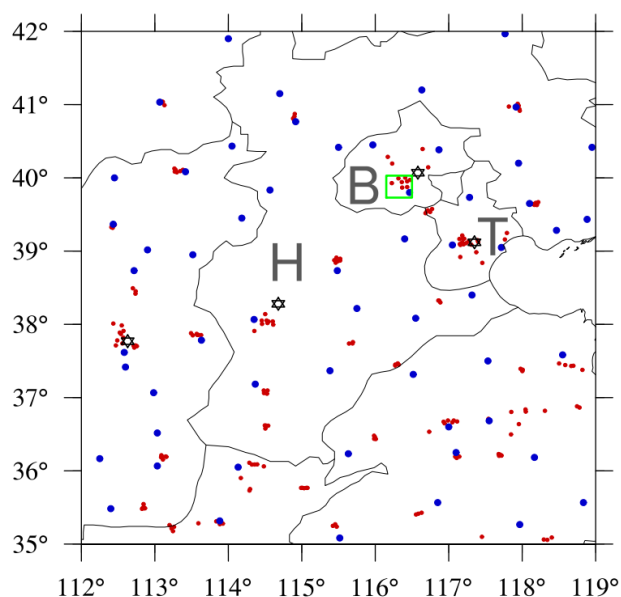
115



## 116 2 Methods

### 117 Data and model configuration

118 The distribution of observed data was shown in Fig. 1. For instance, the meteorological  
119 observations used in this study such as daily maximum temperature, daily mean wind speed, daily  
120 total precipitation were obtained from the China Meteorological Data Service Center (CMA,  
121 <http://data.cma.cn>), with blue dots shown in Fig. 1. Observed surface ozone data are obtained from  
122 China National Environmental Monitoring Centre (<http://www.pm25.in>), with red dots shown in  
123 Fig. 1. Meteorological Assimilation Data Ingest System (MADIS) hourly 2-meter temperature,  
124 specific humidity, 10-meter wind speed and direction are available from The Meteorological  
125 Assimilation Data Ingest System (MADIS; <https://madis.ncep.noaa.gov>), with hexagons shown in  
126 Fig. 1.



127

128 **Fig. 1** Distribution of observational sites over the NCP. (blue dots: daily maximum temperature daily  
129 mean wind speed at 10-meter and daily total precipitation from China Meteorological Administration  
130 (CMA); red dots: O<sub>3</sub> monitoring sites from China National Environmental Monitoring Centre; black  
131 hexagon: hourly temperature at 2-meter (T2), specific humidity at 2-meter (Q2), wind speed (WS10) and  
132 direction (WD10) at 10-meter from MADIS; green box: urban area of Beijing).

133



134 For modeling the meteorological conditions, WRF V3.8.1 is used in this study. The domain is  
135 centered at 110° E, 34° N, with a total of 34 vertical layers and top pressure at 50 hPa. The spatial  
136 resolution is 36 km. The physics parameterizations used in this study are the same as our previous  
137 studies (Gao et al., 2017; Zhang et al., 2019), including the Morrison double moment microphysics  
138 (Morrison et al., 2009), the Rapid Radiative Transfer Model for GCMs (RRTMG) longwave and  
139 shortwave radiation (Iacono et al., 2008; Morcrette et al., 2008), the unified Noah land surface  
140 model (Chen and Dudhia, 2001), the Mellor-Yamada-Janjic planetary boundary layer (PBL)  
141 scheme (Janjić, 1990, 1994; Mellor and Yamada, 1982), and the Grell-Freitas cumulus scheme  
142 (Grell and Freitas, 2014). The initial and boundary conditions were generated from the NCEP  
143 Climate Forecast System Reanalysis (CFSR) version 2 (Saha et al., 2013), with a spatial resolution  
144 of 0.5°×0.5°.

145 For modeling atmospheric chemistry, the widely used Community Multi-scale Air Quality  
146 (CMAQ) model (Byun and Ching, 1999; Byun and Schere, 2006), with the latest version 5.2, was  
147 used in this study. The major gas phase chemistry was represented by the carbon-bond version 6  
148 (CB06) and AERO6 aerosol module. Initial and boundary conditions were from Model for Ozone  
149 and Related chemical Tracers, version 4 (MOZART-4) (Emmons et al., 2010). A dynamical  
150 downscaling tool was developed in this study to link the Mozart output to CMAQ, based upon the  
151 package of Mozart to WRF-Chem (mozbc: [https://www2.aom.ucar.edu/wrf-chem/wrf-chem-](https://www2.aom.ucar.edu/wrf-chem/wrf-chem-tools-community)  
152 [tools-community](https://www2.aom.ucar.edu/wrf-chem/wrf-chem-tools-community)). With this tool, the default clean air profile provided by the CMAQ 5.2 package  
153 was replaced by more realistic boundary variations at both the surface and different vertical levels.  
154 A continuous run from June 1 to July 4 was performed, with the first week discarded as spinup.

155 The anthropogenic emissions of air pollutants in China were estimated by Tsinghua University,  
156 detailed in previous studies (Wang et al., 2014; Zhao et al., 2013; 2017; 2018) and updated based  
157 on the Multiresolution Emission Inventory for China (MEIC, 0.25°×0.25°;  
158 <http://www.meicmodel.org/>) (Li et al., 2017a).

159 The biogenic emissions were calculated by the Model of Emissions of Gases and Aerosols  
160 from Nature version 2.1 (MEGAN; Guenther et al., 2006; Guenther et al., 2012). MEGAN input  
161 data includes three components: plant functional type (PFT), leaf area index (LAI) and emission  
162 factors (EF). There is a total of 19 emission species including isoprene, terpenes, etc., derived  
163 from more than 100 emissions compounds. For each of the 19 species, the emission rates  $F_i$  ( $\mu\text{g}$   
164  $\text{m}^{-2} \text{h}^{-1}$ ) for a certain grid were defined in Eq. 1 with  $i$  denoting the species.



165 
$$F_i = \gamma_i \sum \varepsilon_{i,j} \chi_j \quad (\text{Eq. 1})$$

166 where  $\varepsilon_{i,j}$  and  $\chi_j$  are the emission factor and fractional coverage of plant functional type ( $j$ ) in  
167 each grid respectively.  $\gamma_i$  is the emission activity defined based on light (denoted as L),  
168 temperature (T), leaf age (LA), soil moisture (SM), leaf area index (LAI) and CO<sub>2</sub> inhibition  
169 (denoted as CI), following Eq. 2.

170 
$$\gamma_i = C_{CE} LAI \gamma_{L,i} \gamma_{T,i} \gamma_{LA,i} \gamma_{SM,i} \gamma_{CI,i} \quad (\text{Eq. 2})$$

171 where  $C_{CE}$  is the canopy environment coefficient and 0.57 was used following Guenther et al.  
172 (2012).

173 Compared with the previous version 2.0 with only 4 PFTs, there are 16 types of PFTs  
174 represented in the new MEGAN version (Guenther et al., 2006; Guenther et al., 2012), allowing  
175 for more accurate estimations of PFT-differentiated emission factors. PFT and LAI data were  
176 from the MODIS MCD12Q1 (Friedl et al., 2010) and MCD15A2H datasets (Myneni et al., 2015)  
177 respectively. The 8 vegetation types in MODIS were apportioned to the 16 PFT types in  
178 MEGAN2.1 based on the temperature zone. For example, MODIS has only one type of broad  
179 leaf deciduous trees, while MEGAN 2.1 has three, including broad leaf deciduous tropical,  
180 temperate and boreal trees. The broad leaf deciduous trees in MODIS are mapped onto the three  
181 MEGAN types based on the latitudinal boundaries of the tropical, temperate and boreal zones,  
182 with detailed mapping information provided in Table S4 in the supporting information. Monthly  
183 mean LAIs were used in this study. The meteorological conditions used to generate biogenic  
184 emission in MEGAN were provided by the WRF simulation.

185

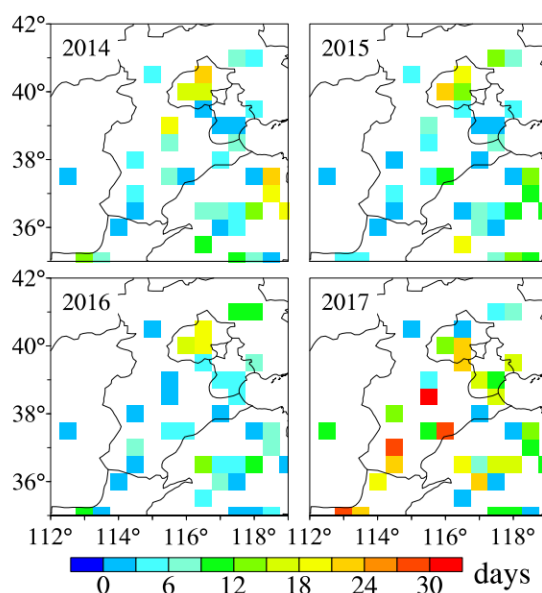
## 186 **3 Results**

### 187 **3.1 Observed ozone features**

188 The Technical Regulation on Ambient Air Quality Index (HJ633-2012) defines six classes of  
189 ozone related pollution based on the daily maximum 8-h ozone concentration (MDA8). Classes I  
190 and II are clean conditions (MDA8 less than 82 ppbv), class III (82-110 ppbv) indicates slight  
191 pollution, class IV (110-135 ppbv) represents medium pollution, and classes V and VI are severe  
192 pollution conditions with MDA8 higher than 135 ppbv. Utilizing the observed MDA8 from



193 China National Environmental Monitoring Centre (<http://www.pm25.in>), we first analyze the  
194 severe and medium ozone pollution events considering their large impact on human health. The  
195 observed MDA8 was interpolated to a  $0.5^\circ \times 0.5^\circ$  grid. Fig. 2 shows the number of severe ozone  
196 pollution days (MDA8 greater than 110 ppbv) during the summer of 2014-2017. The number of  
197 severe ozone pollution days in 2017 is larger than 9 in most areas, which is substantially higher  
198 than that of the other three years when most areas have fewer than 6 days. Frequent occurrence  
199 of severe ozone pollution happens in southern Beijing and south of Hebei Province (the area  
200 marked with letter H in Fig. 1 in the supporting information).



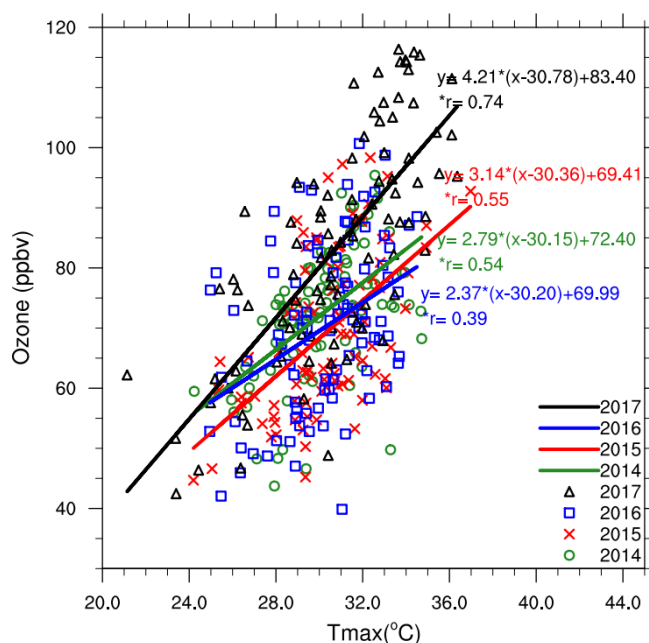
201  
202 **Fig. 2** The number of severe ozone pollution days (MDA8 greater than 110 ppbv) during the  
203 summer of 2014-2017 over NCP.

### 204 205 **3.2 Meteorological factors modulating the high ozone events**

206 Correlation between MDA8 ozone and daily maximum 2-meter temperature (Fig. 3) shows  
207 statistically significant values for all four years, confirming the significant impact of temperature  
208 on ozone. However, the correlation in 2017 is obviously higher than the other three years, and  
209 the regression slope of 4.21 ppbv/°C is about 1.07 to 1.84 ppbv/°C higher than the other three  
210 years, demonstrating the larger impact of temperature in 2017. Both the higher correlation (0.74)  
211 and the larger slope in 2017 are contributed mainly by days with ozone above the top 10% (104



212 ppbv), which are related to the long-lasting high-ozone periods (see Table S1 and Fig. S1) during  
213 June 14-21 and June 26-July 3. Removing data above the top 10% brings the correlation (0.63)  
214 and slope closer to those of the other three years (Fig. S2). Furthermore, the mean temperature in  
215 2017 is not statistically different from that of the other three years, suggesting that the higher  
216 temperature period has disproportionate effects on ozone. Jaffe and Zhang (2017) also found a  
217 larger regression slope between ozone and temperature during the abnormally-warm month of  
218 June 2015 in the western U.S. compared to the previous five years with more normal  
219 temperatures. Please note that tables and figures in the supporting information will be denoted  
220 with S in the following descriptions.  
221

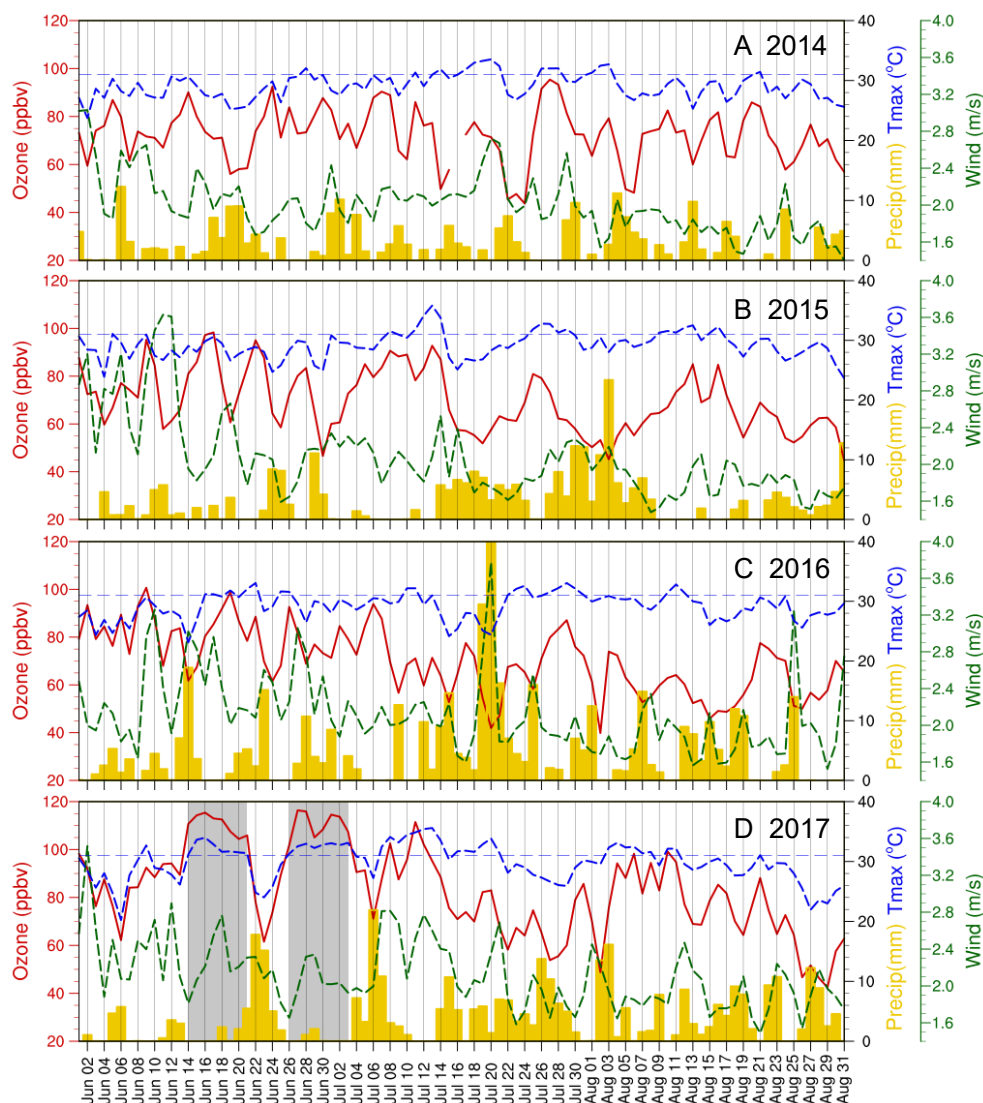


222  
223 **Fig. 3** The correlation between summer MDA8 ozone and daily maximum 2-meter temperature (Tmax)  
224 for 2014-2017 over NCP. Regional mean was calculated from the observational sites over NCP so each  
225 data point corresponds to a regional mean value of MDA8.

226  
227 To further delve into the meteorological factors modulating the ozone variations in the summer  
228 of 2014-2017, the time series of 2017 summer MDA8 ozone is shown in Fig. 4, along with daily  
229 maximum temperature, wind speed and daily total precipitation. From Fig. 4D, the two long-



230 lasting ozone episodic events (event 1: June 14-21 and event 2: June 26-July 3) occur during heat  
231 waves concomitant with stagnant (calm or low wind speed), dry (little or no precipitation) air and  
232 strong solar radiation (not shown), conducive to ozone formation and accumulation. This feature  
233 during the heat wave period was illuminated in Table S2 as well, showing that among all the  
234 observational stations with MDA8 ozone exceeding 110 ppbv, 87% (62%) and 96% (81%) occurs  
235 with daily precipitation less than 1 mm (daily precipitation less than 1 mm and daily mean wind  
236 speed lower than 3 m/s). Long lasting hot and stagnant weather conditions were not clearly  
237 observed during 2014-2016 (Fig. 4A-C).  
238



239

240

241

242

243

244

245

246

247

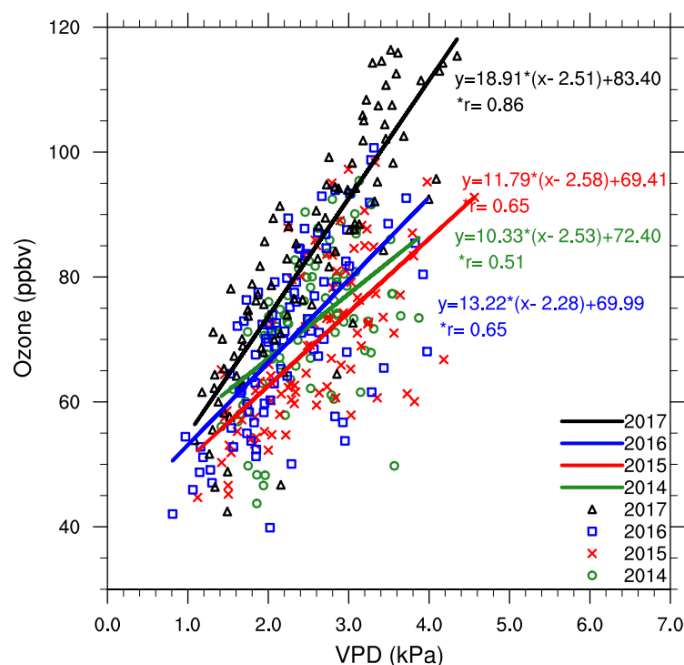
**Fig. 4** Time series of observed MDA8 O<sub>3</sub> (red lines; based on sites from China National Environmental Monitoring Centre; red points in Fig. 1), daily maximum temperature at 2m (blue lines), daily mean wind speed at 10m (green lines) and daily total precipitation (yellow bars) over NCP (based on sites from CMA; blue dots in Fig. 1) during the summer from 2014 to 2017. The regional precipitation was set to zero for a certain day if less than 15% (9 sites) of the total sites (58 sites) with daily total precipitation greater than 1 mm.



### 248 3.3 Effect of land use and biogenic emission on ozone

249 Biogenic emissions contribute importantly to ozone formation. The MEGAN model has been  
250 widely used to simulate biogenic emissions in air quality modeling studies (Guenther et al., 2012),  
251 but recent research suggested that biogenic emissions may be underestimated in the model for  
252 several reasons:

253 *a)* Water-stressed impact on biogenic emissions. Zhang and Wang (2016) found that two high  
254 ozone events in the U.S. were associated with excess isoprene release due to dry and hot weather  
255 conditions that induced water stress in plants. The increased vapor pressure deficit (VPD; the  
256 pressure difference between saturation vapor and ambient vapor) drives the release of more  
257 isoprene but the VPD effect on biogenic emissions has not been taken into consideration in  
258 MEGAN 2.1, so the subsequent influence of biogenic emissions on ozone may be largely  
259 underestimated. Zhang and Wang (2016) suggested a doubling of daily biogenic isoprene when  
260 the daily VPD reaches 1.7 kPa or greater. The monthly mean VPD spatial distribution in June 2017  
261 (Fig. S3) as well as the high correlation between observed MDA8 ozone and VPD (Fig. 5) suggests  
262 enhanced isoprene emission in NCP so we will test this VPD mechanism using model simulations.



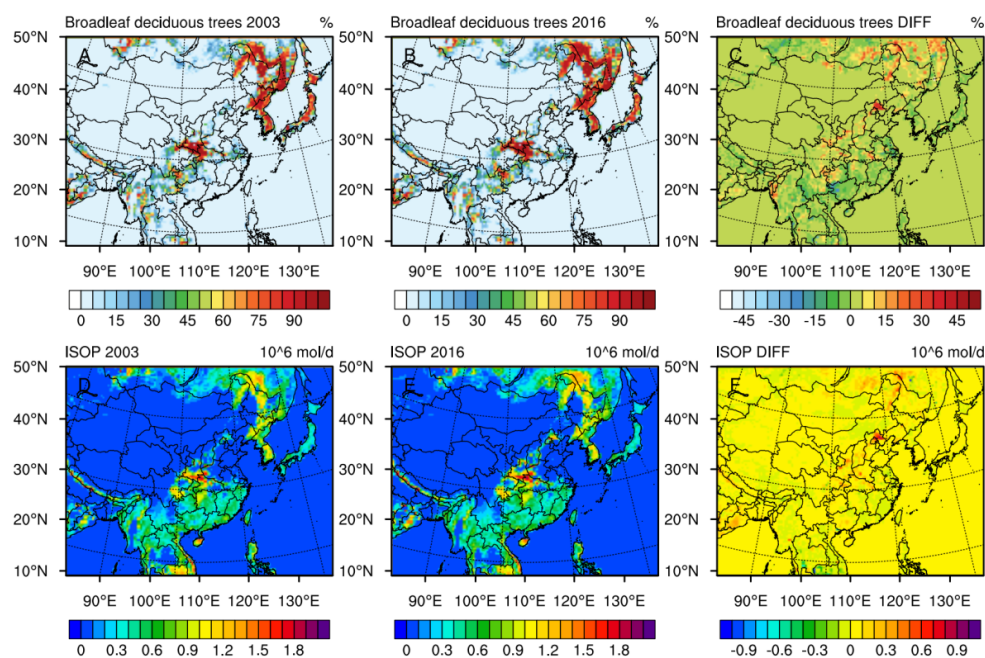
263



264 **Fig. 5** The correlation between summer MDA8 ozone and daily maximum VPD during 2014-2017  
265 over NCP. Regional mean was calculated from the observational sites over NCP so each data point  
266 corresponds to a regional mean value of MDA8.

267

268 *b)* Changes in land cover may affect biogenic emissions. As reflected by the much higher  
269 emission factor, biogenic isoprene emission is enhanced in broad leaf forest relative to other land  
270 cover types such as needle leaf forest, shrub, grass or crop (Table 2 in Guenther et al. (2012)). In  
271 NCP, broad leaf tree is the dominant land cover type and its coverage has been increasing  
272 dramatically since the 1970s, primarily a result of the “Three-North Protection Forest System”  
273 project. For example, based on Moderate Resolution Imagine Spectroradiometer (MODIS) land  
274 use data (Friedl et al., 2010), the coverage of broadleaf deciduous temperate tree nearly doubled  
275 from 2003 to 2016 over NCP (top row of Fig. 6). This has resulted in a substantial increase of  
276 isoprene emissions between 2003 and 2016 (Fig. 6), particularly north of the Beijing, Hebei and  
277 Tianjin, where the increase is more than 200%. It is vital to quantify the effect of land cover  
278 changes on biogenic emissions such as isoprene and the subsequent impact on ozone formation.



279

280



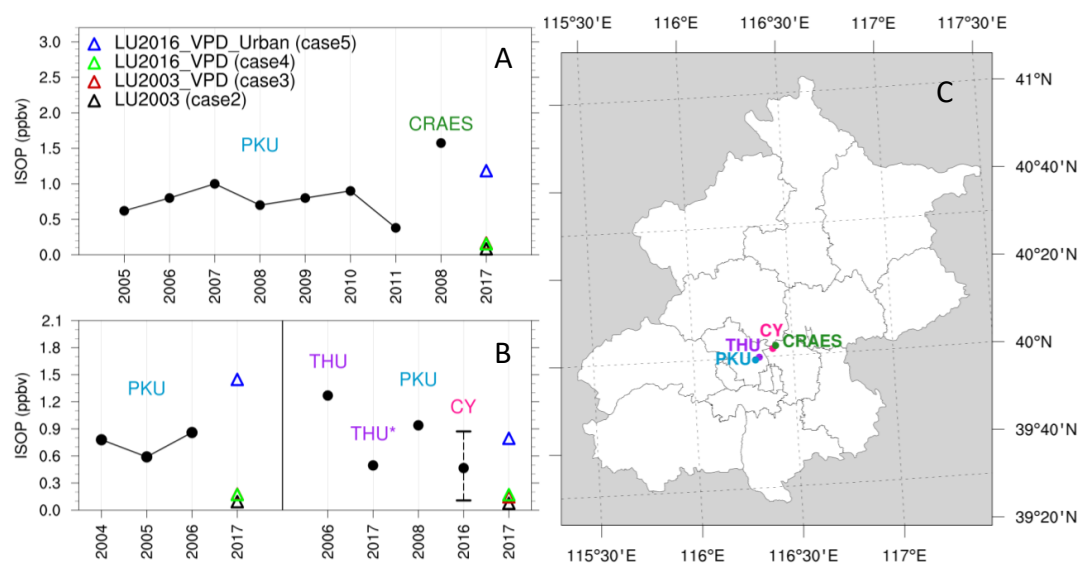
281 **Fig. 6** Spatial distribution of broadleaf deciduous trees in 2003 (Fig. 6A), 2016 (Fig. 6B) and their  
282 differences (2016-2003; Fig. 6C), and the biogenic isoprene emissions during the heat waves periods (June  
283 14-21 2017; June 26-July 3rd 2017) based on the land cover in 2003 (Fig. 6D), 2016 (Fig. 6E) and their  
284 differences (2016-2003; Fig. 6F).

285 c) Impact of urban landscape on biogenic emission. Land use type cataloged in the MODIS  
286 MCD12Q1 product (Friedl et al., 2010) does not take into consideration urban green spaces, which  
287 may lead to a 15% underestimation of total BVOC emissions in 2015 over Beijing (Ren et al.,  
288 2017). Generally, urban ozone production is highly sensitive to VOC emissions (Xing et al., 2011;  
289 Liu et al., 2012). Bell and Ellis (2004) found a doubling of ozone in urban area relative to rural  
290 areas for the same percentage increase of biogenic emissions. The impact of biogenic emission  
291 from urban landscape on urban ozone formation has not been considered in previous studies. For  
292 sensitivity analysis, we added a 15% increase of the total BVOCs emissions in Beijing to  
293 investigate its impact on urban ozone formation. These emissions were distributed evenly in the  
294 urban core area of Beijing as the increase of biogenic emissions from urban landscape were only  
295 available for Beijing.

296 To elucidate the mechanism modulating the ozone events discussed above, the regional  
297 meteorology and air quality model WRF/CMAQ was used to conduct simulations during June 8  
298 to July 4 2017. The WRF simulations generally meet the benchmark standard for meteorological  
299 variables (Table S3). For air quality simulations, five scenarios were designed, with biogenic  
300 emissions ignored in the base case. Compared to the base case, case 2 adds biogenic emission  
301 associated with the land cover of 2003, and cases 3, 4 and 5 are the same as case 2 except for the  
302 inclusion of the VPD effect, both VPD and land cover of 2016, and VPD and land cover of 2016  
303 combined with the effect of urban green spaces, respectively. To validate the reasonableness of  
304 adding the biogenic emission, we first evaluate the simulated isoprene concentration, one of the  
305 most important species closely related to ozone formation, from WRF/CMAQ among different  
306 cases. Since there is a lack of observed ambient isoprene concentration during this study period,  
307 the data available (mostly over Beijing) from the literature was retrieved and used as cross  
308 comparison with the model results (Fig. 7). From Fig. 7A,B, the observed mean isoprene  
309 concentration ranges from 0.4 ppbv to 1.6 ppbv in various sites of Beijing. The model simulations  
310 by taking into consideration of isoprene emissions from VPD, land cover of 2016 and urban green  
311 spaces (case 5) yield the best performance, with isoprene concentration of 0.8 ppbv to 1.4 ppbv.



312 However, the other cases (with isoprene concentrations of 0.1 ppbv to 0.2 ppbv) substantially  
313 underestimate the isoprene concentrations. Therefore, the isoprene emissions from urban green  
314 spaces (comparing case 5 and case 4) in Beijing plays a vital role in the isoprene concentrations,  
315 which subsequently affect the ozone formation which will be further evaluated and discussed  
316 below.



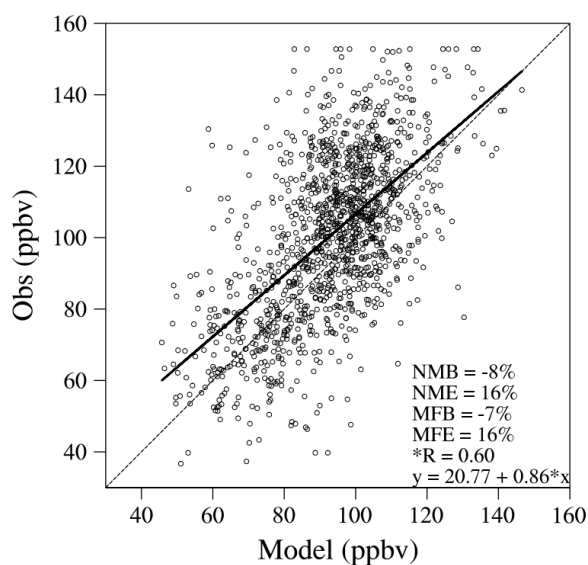
317

318 **Fig. 7** The comparison of isoprene concentrations between model simulations and observations in Beijing.  
319 The black dots represent the observed data from various of literatures, whereas the hollow triangles (in  
320 black, red, green and blue) represent the model simulations for the four cases described above (cases 2-5).  
321 For each observational dataset, the corresponding reference number was labelled on the right of the site  
322 name in Fig. 7A,B, with site locations shown in Fig. 7C. One exception is the unpublished work in THU\*  
323 which is from the observations using proton-transfer-reaction time-of-flight mass spectrometer (PTR-ToF-  
324 MS) conducted by Tsinghua University (manuscript in preparation). Please note that no observation period  
325 matches exactly our simulation time, making the comparison more qualitative rather than quantitative.  
326 However, the model evaluation did match the respective location and time (i.e., day-time or selected hour)  
327 among different observations. The model simulation period used in the comparison is from June 8 to July  
328 4, 2017. For observations, in Fig. 7A, the dots represent the mean isoprene concentrations during day-time  
329 in August from 2005 to 2011 at Peking University (PKU; (Zhang et al., 2014); left of Fig. 7A) and from 16  
330 July to 18 August 2008 at Chinese Research Academy of Environmental Science (CRAES; (Yang et al.,  
331 2018); right of Fig. 7A). In Fig. 7B, the dots on the left represent the mean isoprene concentration of hour  
332 8:00 and hour 16:00 (local standard time) in August from 2004-2006 (with detailed measurement time  
333 shown in Table 1 of (Shao et al., 2009)) in PKU. The observational data on the right of Fig. 7B is on daily  
334 mean scale during a certain period (with one site of CY showing minimal and maximal daily mean values  
335 during the period) from four sources. The two leftmost dots are located at the campus of Tsinghua  
336 University (THU), with one from August 15-20 2006 (Duan et al., 2008) and the other from July 14 to  
337 August 5 2017 (manuscript in preparation as explained above). The third dot represents data measured at



338 PKU from July 24 to August 27, 2008 (Liu et al., 2015) and the fourth dot indicates data observed at  
339 Chaoyang District (CY; (Gu et al., 2019)).

340 Since the effect of urban landscape was only applied to Beijing in case 5, we use case 4  
341 (combination of VPD and land cover change effects) (referred to as B\_MDA8) as the reference.  
342 Therefore, we first compare MDA8 ozone in case 4 with observations and reasonable performance  
343 is achieved with MFB/MFE of -7%/16% (Fig. 8). Considering the mean bias likely attributed to  
344 the factors such as emission uncertainty or model inherent biases, thus a bias correction was  
345 applied to each case by adding 7% of mean observed MDA8 ozone during June 8–July 4 2017.



346

347 **Fig. 8** MDA8 ozone evaluation of over NCP during June 8 to July 4 in 2017.

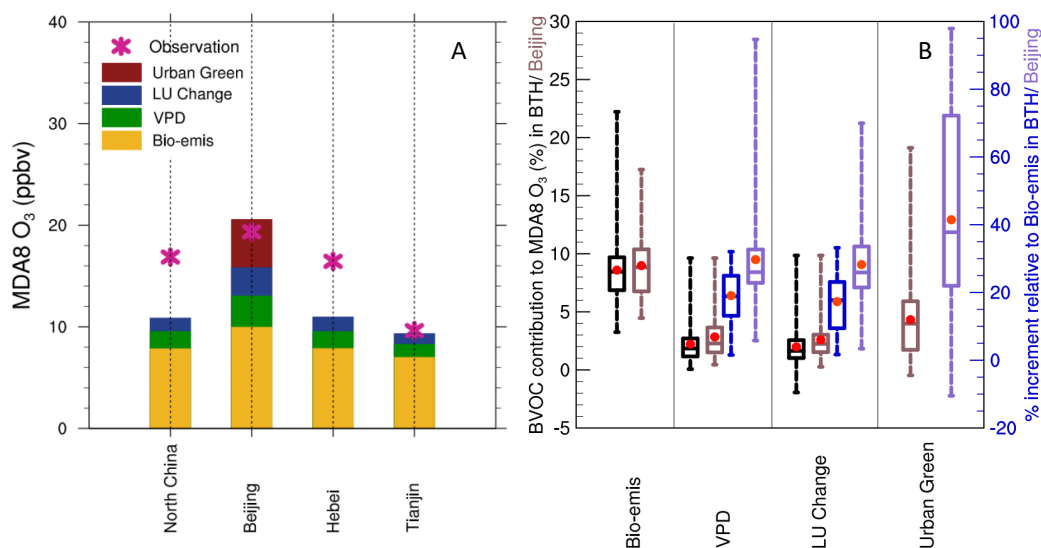
348

349 Zooming into the two ozone episodic events (June 14–21, June 26–July 3), the mean MDA8  
350 values of case 4 are 98.02 ppbv, 108.89 ppbv, 95.75 ppbv, and 98.98 ppbv for NCP, Beijing, Hebei  
351 and Tianjin, respectively, during the heat wave periods (June 14–21, 2017; June 26–July 3, 2017),  
352 whereas the MDA8 ozone value for the case (case 1) without biogenic emission are 87.15 ppbv,  
353 93.06 ppbv, 84.78 ppbv and 89.65 ppbv for the corresponding region. The ozone increment from  
354 case 2 to case 5 (as well as observations; magenta stars in Fig. 9A) relative to case 1 was shown in  
355 Fig. 9A for these regions. Including biogenic emission based on the land cover of 2003 (case 2)  
356 yields an extra mean MDA8 ozone of 7.84 ppbv (8% of B\_MDA8), 9.96 ppbv (9% of B\_MDA8),



357 7.86 ppbv (8% of B\_MDA8) and 6.99 ppbv (7% of B\_MDA8) for NCP, Beijing, Hebei and Tianjin,  
358 respectively (yellow bars in Fig. 9A), compared to case 1. Including the VPD effect (case 3) adds  
359 an extra mean MDA8 of 1.71 ppbv in NCP compared to case 2, and the enhancement is highest in  
360 Beijing (3.08 ppbv) (green bars in Fig. 9A). Additional MDA8 ozone enhancement is simulated  
361 by including the effect of land cover change (increase in natural broadleaf forest; top row in Fig.  
362 6; case 4), i.e., an extra MDA8 of 1.32 ppbv in NCP relative to case 3, with the highest contribution  
363 of 2.79 ppbv in Beijing (blue bars in Fig. 9A). The urban landscape (case 5) in Beijing yields an  
364 extra 4.74 ppbv or 4% of MDA8 compared to case 4, almost doubling the effect of VPD and land  
365 cover change in Beijing. The larger percentage increase in MDA8 ozone (41% from Fig. 9A, which  
366 will be discussed in Fig. 9B as well) due to urban landscape relative to the prescribed 15% increase  
367 in BVOC emission in Beijing supports the notion of an amplified MDA8 ozone response in urban  
368 areas because of the high sensitivity of ozone to VOC emissions, which well matches observational  
369 data (magenta star).

370 To further illustrate the contributions of BVOC to MDA8, Fig. 9B shows the contribution of  
371 biogenic emissions (Bio\_emis, based on land cover of 2003), VPD, land cover change, and urban  
372 landscape (or urban green) to MDA8 as a fraction of the MDA8 of B\_MDA8 (left y-axis in Fig.  
373 9B) and as percentage increment relative to the MDA8 contributed by biogenic emissions in case  
374 2 (right y-axis in Fig. 9B) in BTH (Beijing, Tianjin, Hebei; with letters B, T and H marked in Fig.  
375 1) and Beijing. For BTH, the mean contribution to B\_MDA8 is 9%, 2% and 2% for Bio\_emis,  
376 VPD and land cover change (red dots in the black bars in Fig. 9B), respectively, with maximum  
377 contributions of 22%, 10% and 10%. For Beijing, the contributions of Bio\_emis, VPD, land cover  
378 change, and urban landscape are 9%, 3%, 3% and 4% respectively (red dots in the brown bars in  
379 Fig. 9B). Urban landscape (19%) contributes more than Bio\_emis (17%) in the urban area of  
380 Beijing in terms of the maximal contribution (maximum value of the brown box in Fig. 9B).  
381 Compared with Bio\_emis, the mean increments are 19% and 17% for VPD and land cover change  
382 (red dots in the blue bars in Fig. 9B). For Beijing, the mean additional enhancements are 30%, 28%  
383 and 41% for VPD, land cover change and urban landscape relative to Bio\_emis (red dots in the  
384 purple bars in Fig. 9B), with a combined increment of 99% compared to the MDA8 ozone  
385 contributed by biogenic emission based on the land cover of 2003. Although only grid cells with  
386 both simulations and observations available are used in Fig. 9B, the results are similar if all model  
387 grids points were used (not shown).



388

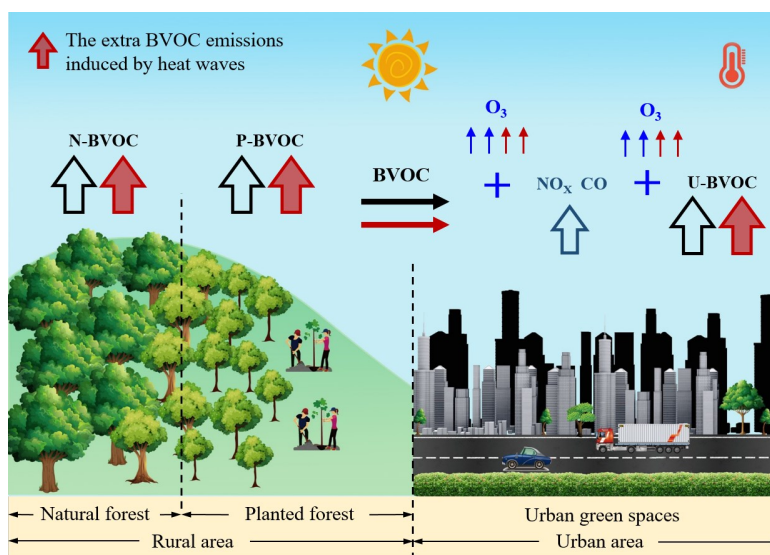
389 **Fig. 9** Biogenic contribution to MDA8 ozone during the heat wave periods (June 14-21; June 26-July 3),  
390 shown by the individual (left) and percentage contribution (right) of standard biogenic emissions using  
391 MEGAN 2.1 with the land cover of 2003 (Bio-emis), VPD effect, land cover (LC) change and urban green  
392 spaces. The color bars (Fig. 9A) represent the simulated contributions of biogenic emissions (yellow), VPD  
393 (green), land use changes (blue), and urban green (red) to the MDA8 ozone concentrations in NCP, Beijing,  
394 Hebei and Tianjin respectively. The magenta stars in Fig. 9A represent the observed biogenic emissions  
395 calculated by subtracting the contribution to MDA8 ozone simulated in the base case from the observed  
396 total MDA8 ozone. The box-and-whisker plot shows the contribution of biogenic emissions, VPD, land  
397 cover change and urban green spaces to the total MDA8 ozone in BTH (black) and Beijing (brown) (y-axis  
398 on the left), and the percentage increment (right y-axis) of VPD, land cover change and urban green  
399 relative to MDA8 induced by Bio-emis for BTH (blue) and Beijing (purple). Please note that urban green  
400 spaces are only available for Beijing. The top and bottom edges of the boxes represent the 75 and 25 percentiles,  
401 with the centered line and red dot showing the median and mean, respectively.

402 Herein the mechanisms for ozone enhancement are summarized in the schematic of Fig. 10.  
403 Both natural and anthropogenic emissions contribute to ozone formation. Because of the “Three-  
404 North Protection Forest System” project, natural forest north of Beijing has more than tripled in  
405 area coverage compared to 2003, leading to an increasing trend in biogenic emissions. Under heat  
406 wave conditions, biogenic emissions may be further enhanced through the effect of VPD in  
407 addition to the effect of temperature. For urban areas, even more biogenic emissions may be



408 emitted from urban landscape. All these mechanisms for increasing biogenic emissions could  
409 enhance ozone formation, particularly over urban areas such as Beijing.

410



411

412 **Fig. 10** A schematic diagram of the impact of biogenic emission on ozone formation. N-BVOC refers to  
413 natural biogenic emission, P-BVOC refers to the biogenic emission from planted forest and in this study  
414 representing the increase of forest coverage. U-BVOC refers to urban biogenic VOCs generated from urban  
415 green spaces. The red thick upward arrows indicate extra VOCs may be induced by the heat waves.

416

#### 417 **4 Discussion**

418 The mechanisms contributing to the severe ozone pollution events in the summer of 2017 in  
419 NCP were investigated. Two severe tropospheric ozone pollution events occurred in the NCP  
420 during the periods of June 14 to 21 and June 26 to July 3. We provided support for the roles of the  
421 observed meteorological conditions including high temperature and stagnant dry weather, which  
422 favor high ozone concentrations. More importantly, the influence of biogenic emissions on ozone  
423 formation was investigated in more detail by incorporating important biogenic emission factors  
424 that are typically ignored in regional model simulations. Biogenic emissions based on the land  
425 cover of 2003 yields an extra mean MDA8 ozone of 7.84 ppbv for the NCP. Including the VPD  
426 effect and land cover change adds 1.71 ppbv and 1.32 ppbv of ozone in the NCP. These



427 contributions are even larger in Beijing, with VPD adding 3.08 ppbv and land cover change adding  
428 2.79 ppbv. Most notably, biogenic emissions from urban landscape (i.e., green spaces) have so far  
429 not been considered in ozone regional modeling studies to our knowledge. By adding this source  
430 in the urban area of Beijing, substantial ozone enhancement was simulated, bringing the  
431 WRF/CMAQ simulation of MDA8 closer to observations. The urban landscape in Beijing yields  
432 an extra 4.74 ppbv of MDA8, comparable to the combined effect of VPD and land cover change  
433 in Beijing. Together, the combined effect of VPD, land cover change, and urban landscape doubles  
434 the effect of biogenic emission calculated based on the land cover of 2003 and not including the  
435 VPD and urban landscape effects.

436 The BVOC emissions from urban green spaces are projected to increase by more than two times  
437 in 2050 due to urban area expansion (Ren et al., 2017). Together with the more frequent heat waves  
438 projected for the future (Gao et al., 2012; Zhang et al., 2018), the impact of biogenic emissions on  
439 ozone pollution in the NCP will likely play an increasingly important role in ozone pollution and  
440 should be taken into considerations in future air quality management plans to address issues of air  
441 quality and health. The effect of urban green spaces was only considered in Beijing in this study  
442 as we lack the data to parameterize this effect in other regions. Considering the substantial effect  
443 of urban green spaces on urban ozone formation, it is vital to evaluate similar effects in other cities  
444 where ozone pollution is a concern.

445

446 **Competing interests.** The authors declare that they have no conflict of interest.

447 **Acknowledgement.** This research was supported by grants from the National Key Project  
448 of MOST (2017YFC1404101), National Natural Science Foundation of China (41705124,  
449 21625701, 41722501, 91544212), Shandong Provincial Natural Science Foundation, China  
450 (ZR2017MD026) and Fundamental Research Funds for the Central Universities (201712006). Y.  
451 Wang was supported by the National Science Foundation Atmospheric Chemistry Program.  
452 PNNL is operated for DOE by Battelle Memorial Institute under contract DE-AC05-76RL01830.

453



454 **Author contributions.** YG came up with the original idea and YG, YW and CL designed the  
455 research. MM conducted all the analysis, SZ, LRL, SW, BZ, XC, HS, TZ, LS, XY and HW  
456 wrote the paper.

#### 457 **References:**

458 Avnery, S., Mauzerall, D. L., Liu, J. F., and Horowitz, L. W.: Global crop yield reductions due to  
459 surface ozone exposure: 1. Year 2000 crop production losses and economic damage, Atmos  
460 Environ, 45, 2284-2296, [10.1016/j.atmosenv.2010.11.045](https://doi.org/10.1016/j.atmosenv.2010.11.045), 2011.

461 Bell, M., and Ellis, H.: Sensitivity analysis of tropospheric ozone to modified biogenic emissions  
462 for the Mid-Atlantic region, Atmos Environ, 38, 1879-1889, 2004.

463 Byun, D., and Ching, J. K. S.: Science Algorithms of the EPA Models-3 Community Multiscale  
464 Air Quality (CMAQ) Modeling System., U. S. Environmental Protection Agency, Office of  
465 Research and Development, EPA, Washington, DC, 727, 1999.

466 Byun, D., and Schere, K. L.: Review of the governing equations, computational algorithms, and  
467 other components of the models-3 Community Multiscale Air Quality (CMAQ) modeling  
468 system, Appl Mech Rev, 59, 51-77, [10.1115/1.2128636](https://doi.org/10.1115/1.2128636), 2006.

469 Chen, F., and Dudhia, J.: Coupling an advanced land surface-hydrology model with the Penn  
470 State-NCAR MM5 modeling system. Part I: Model implementation and sensitivity, Mon  
471 Weather Rev, 129, 569-585, [10.1175/1520-0493\(2001\)129<0569:caalsh>2.0.co;2](https://doi.org/10.1175/1520-0493(2001)129<0569:caalsh>2.0.co;2), 2001.

472 Chen, L., Guo, B., Huang, J. S., He, J., Wang, H. F., Zhang, S. Y., and Chen, S. X.: Assessing  
473 air-quality in Beijing-Tianjin-Hebei region: The method and mixed tales of PM<sub>2.5</sub> and O<sub>3</sub>, Atmos  
474 Environ, 193, 290-301, 2018a.

475 Chen, W. H., Guenther, A. B., Wang, X. M., Chen, Y. H., Gu, D. S., Chang, M., Zhou, S. Z.,  
476 Wu, L. L., and Zhang, Y. Q.: Regional to global biogenic isoprene emission responses to  
477 changes in vegetation from 2000 to 2015, J Geophys Res-Atmos, 123, 3757-3771,  
478 [10.1002/2017jd027934](https://doi.org/10.1002/2017jd027934), 2018b.

479 Chen, Z., Zhuang, Y., Xie, X., Chen, D., Cheng, N., Yang, L., and Li, R.: Understanding long-  
480 term variations of meteorological influences on ground ozone concentrations in Beijing during  
481 2006-2016, Environ Pollut, 245, 29-37, [10.1016/j.envpol.2018.10.117](https://doi.org/10.1016/j.envpol.2018.10.117), 2019.

482 Cheng, Y. F., Zheng, G. J., Wei, C., Mu, Q., Zheng, B., Wang, Z. B., Gao, M., Zhang, Q., He, K.  
483 B., Carmichael, G., Poschl, U., and Su, H.: Reactive nitrogen chemistry in aerosol water as a  
484 source of sulfate during haze events in China, Sci Adv, 2, 2016.



- 485 Duan, J. C., Tan, J. H., Yang, L., Wu, S., and Hao, J. M.: Concentration, sources and ozone  
486 formation potential of volatile organic compounds (VOCs) during ozone episode in Beijing,  
487 Atmos Res, 88, 25-35, 2008.
- 488 Emberson, L. D., Buker, P., Ashmore, M. R., Mills, G., Jackson, L. S., Agrawal, M.,  
489 Atikuzzaman, M. D., Cinderby, S., Engardt, M., Jamir, C., Kobayashi, K., Oanh, N. T. K.,  
490 Quadir, Q. F., and Wahid, A.: A comparison of North American and Asian exposure-response  
491 data for ozone effects on crop yields, Atmos Environ, 43, 1945-1953,  
492 10.1016/j.atmosenv.2009.01.005, 2009.
- 493 Emmons, L. K., Walters, S., Hess, P. G., Lamarque, J. F., Pfister, G. G., Fillmore, D., Granier,  
494 C., Guenther, A., Kinnison, D., Laepple, T., Orlando, J., Tie, X., Tyndall, G., Wiedinmyer, C.,  
495 Baughcum, S. L., and Kloster, S.: Description and evaluation of the Model for Ozone and  
496 Related chemical Tracers, version 4 (MOZART-4), Geosci Model Dev, 3, 43-67, 10.5194/gmd-  
497 3-43-2010, 2010.
- 498 Fiore, A. M., Naik, V., and Leibensperger, E. M.: Air quality and climate connections, J Air  
499 Waste Manage, 65, 645-685, 10.1080/10962247.2015.1040526, 2015.
- 500 Friedl, M. A., Sulla-Menashe, D., Tan, B., Schneider, A., Ramankutty, N., Sibley, A., and  
501 Huang, X. M.: MODIS Collection 5 global land cover: Algorithm refinements and  
502 characterization of new datasets, Remote Sens Environ, 114, 168-182, 2010.
- 503 Fu, J. S., Dong, X., Gao, Y., Wong, D. C., and Lam, Y. F.: Sensitivity and linearity analysis of  
504 ozone in East Asia: The effects of domestic emission and intercontinental transport, J Air Waste  
505 Manage, 62, 1102-1114, 2012.
- 506 Fu, Y., and Liao, H.: Impacts of land use and land cover changes on biogenic emissions of  
507 volatile organic compounds in China from the late 1980s to the mid-2000s: Implications for  
508 tropospheric ozone and secondary organic aerosol, Tellus B, 66, ARTN 24987  
509 10.3402/tellusb.v66.24987, 2014.
- 510 Gao, Y., Fu, J. S., Drake, J. B., Liu, Y., and Lamarque, J. F.: Projected changes of extreme  
511 weather events in the eastern United States based on a high resolution climate modeling system,  
512 Environ Res Lett, 7, 2012.
- 513 Gao, Y., Fu, J. S., Drake, J. B., Lamarque, J. F., and Liu, Y.: The impact of emission and climate  
514 change on ozone in the United States under representative concentration pathways (RCPs),  
515 Atmos Chem Phys, 13, 9607-9621, 10.5194/acp-13-9607-2013, 2013.
- 516 Gao, Y., Leung, L. R., Zhao, C., and Hagos, S.: Sensitivity of US summer precipitation to model  
517 resolution and convective parameterizations across gray zone resolutions, J Geophys Res-Atmos,  
518 122, 2714-2733, 2017.



- 519 Ghirardo, A., Xie, J. F., Zheng, X. H., Wang, Y. S., Grote, R., Block, K., Wildt, J., Mentel, T.,  
520 Kiendler-Scharr, A., Hallquist, M., Butterbach-Bahl, K., and Schnitzler, J. P.: Urban stress-  
521 induced biogenic VOC emissions and SOA-forming potentials in Beijing, *Atmos Chem Phys*,  
522 16, 2901-2920, 10.5194/acp-16-2901-2016, 2016.
- 523 Grell, G. A., and Freitas, S. R.: A scale and aerosol aware stochastic convective parameterization  
524 for weather and air quality modeling, *Atmos Chem Phys*, 14, 5233-5250, 10.5194/acp-14-5233-  
525 2014, 2014.
- 526 Gu, Y. Y., Li, Q. Q., Wei, D., Gao, L. R., Tan, L., Su, G. J., Liu, G. R., Liu, W. B., Li, C. Q., and  
527 Wang, Q. L.: Emission characteristics of 99 NMVOCs in different seasonal days and the  
528 relationship with air quality parameters in Beijing, China, *Ecotox Environ Safe*, 169, 797-806,  
529 2019.
- 530 Guenther, A., Karl, T., Harley, P., Wiedinmyer, C., Palmer, P. I., and Geron, C.: Estimates of  
531 global terrestrial isoprene emissions using MEGAN (Model of Emissions of Gases and Aerosols  
532 from Nature), *Atmos Chem Phys*, 6, 3181-3210, DOI 10.5194/acp-6-3181-2006, 2006.
- 533 Guenther, A. B., Jiang, X., Heald, C. L., Sakulyanontvittaya, T., Duhl, T., Emmons, L. K., and  
534 Wang, X.: The Model of Emissions of Gases and Aerosols from Nature version 2.1  
535 (MEGAN2.1): An extended and updated framework for modeling biogenic emissions, *Geosci  
536 Model Dev*, 5, 1471-1492, 2012.
- 537 Han, X., Zhu, L. Y., Wang, S. L., Meng, X. Y., Zhang, M. G., and Hu, J.: Modeling study of  
538 impacts on surface ozone of regional transport and emissions reductions over North China Plain  
539 in summer 2015, *Atmos Chem Phys*, 18, 12207-12221, 2018.
- 540 Iacono, M. J., Delamere, J. S., Mlawer, E. J., Shephard, M. W., Clough, S. A., and Collins, W.  
541 D.: Radiative forcing by long-lived greenhouse gases: Calculations with the AER radiative  
542 transfer models, *J Geophys Res-Atmos*, 113, D13103, 10.1029/2008jd009944, 2008.
- 543 Jacob, D. J., and Winner, D. A.: Effect of climate change on air quality, *Atmos Environ*, 43, 51-  
544 63, 10.1016/j.atmosenv.2008.09.051, 2009.
- 545 Jaffe, D. A., and Zhang, L.: Meteorological anomalies lead to elevated O<sub>3</sub> in the western U. S. in  
546 June 2015, *Geophys Res Lett*, 44, 1990-1997, 2017.
- 547 Janjić, Z. I.: The step-mountain coordinate: Physical package, *Mon Weather Rev*, 118, 1429-  
548 1443, 10.1175/1520-0493(1990)118<1429:tsmcpp>2.0.co;2, 1990.
- 549 Janjić, Z. I.: The Step-Mountain Eta Coordinate Model: Further developments of the convection,  
550 viscous sublayer, and turbulence closure schemes, *Mon Weather Rev*, 122, 927-945,  
551 10.1175/1520-0493(1994)122<0927:TSMECM>2.0.CO;2, 1994.



- 552 Li, K., Jacob, D. J., Liao, H., Shen, L., Zhang, Q., and Bates, K. H.: Anthropogenic drivers of  
553 2013-2017 trends in summer surface ozone in China, *Proc Natl Acad Sci USA*,  
554 10.1073/pnas.1812168116, 2019.
- 555 Li, M., Zhang, Q., Kurokawa, J., Woo, J. H., He, K. B., Lu, Z. F., Ohara, T., Song, Y., Streets,  
556 D. G., Carmichael, G. R., Cheng, Y. F., Hong, C. P., Huo, H., Jiang, X. J., Kang, S. C., Liu, F.,  
557 Su, H., and Zheng, B.: MIX: A mosaic Asian anthropogenic emission inventory under the  
558 international collaboration framework of the MICS-Asia and HTAP, *Atmos Chem Phys*, 17,  
559 935-963, 10.5194/acp-17-935-2017, 2017a.
- 560 Li, R., Cui, L. L., Li, J. L., Zhao, A., Fu, H. B., Wu, Y., Zhang, L. W., Kong, L. D., and Chen, J.  
561 M.: Spatial and temporal variation of particulate matter and gaseous pollutants in China during  
562 2014-2016, *Atmos Environ*, 161, 235-246, 10.1016/j.atmosenv.2017.05.008, 2017b.
- 563 Liu, F., Zhang, Q., A., R. J. v. d., Zheng, B., Tong, D., Yan, L., Zheng, Y., and He, K.: Recent  
564 reduction in NO<sub>x</sub> emissions over China: Synthesis of satellite observations and emission  
565 inventories, *Environ Res Lett*, 11, 114002, 2016.
- 566 Liu, Y., Yuan, B., Li, X., Shao, M., Lu, S., Li, Y., Chang, C. C., Wang, Z., Hu, W., Huang, X.,  
567 He, L., Zeng, L., Hu, M., and Zhu, T.: Impact of pollution controls in Beijing on atmospheric  
568 oxygenated volatile organic compounds (OVOCs) during the 2008 Olympic Games: observation  
569 and modeling implications, *Atmos Chem Phys*, 15, 3045-3062, 2015.
- 570 Liu, Z., Wang, Y., Gu, D., Zhao, C., Huey, L. G., Stickel, R., Liao, J., Shao, M., Zhu, T., Zeng,  
571 L., Amoroso, A., Costabile, F., Chang, C. C., and Liu, S. C.: Summertime photochemistry during  
572 CAREBeijing-2007: RO<sub>x</sub> budgets and O<sub>3</sub> formation, *Atmos Chem Phys*, 12, 7737-7752,  
573 10.5194/acp-12-7737-2012, 2012.
- 574 Lu, X., Hong, J. Y., Zhang, L., Cooper, O. R., Schultz, M. G., Xu, X. B., Wang, T., Gao, M.,  
575 Zhao, Y. H., and Zhang, Y. H.: Severe surface ozone pollution in China: A global perspective,  
576 *Environ Sci Tech Lett*, 5, 487-494, 2018.
- 577 Mellor, G. L., and Yamada, T.: Development of a turbulence closure model for geophysical fluid  
578 problems, *Rev Geophys*, 20, 851-875, 1982.
- 579 Morcrette, J. J., Barker, H. W., Cole, J. N. S., Iacono, M. J., and Pincus, R.: Impact of a new  
580 radiation package, McRad, in the ECMWF Integrated Forecasting System, *Mon Weather Rev*,  
581 136, 4773-4798, 10.1175/2008mwr2363.1, 2008.
- 582 Morrison, H., Thompson, G., and Tatarskii, V.: Impact of cloud microphysics on the  
583 development of trailing stratiform precipitation in a simulated squall line: Comparison of one-  
584 and two-moment schemes, *Mon Weather Rev*, 137, 991-1007, 10.1175/2008MWR2556.1, 2009.



- 585 Myneni, R., Knyazikhin, Y., and Park, T.: MCD15A2H MODIS/Terra+Aqua Leaf Area  
586 Index/FPAR 8-day L4 Global 500m SIN Grid V006, in, NASA EOSDIS Land Processes DAAC,  
587 <https://doi.org/10.5067/MODIS/MCD15A2H.006>, 2015.
- 588 Otero, N., Sillmann, J., Schnell, J. L., Rust, H. W., and Butler, T.: Synoptic and meteorological  
589 drivers of extreme ozone concentrations over Europe, *Environ Res Lett*, 11, 024005, 2016.
- 590 Pu, X., Wang, T. J., Huang, X., Melas, D., Zanis, P., Papanastasiou, D. K., and Poupkou, A.:  
591 Enhanced surface ozone during the heat wave of 2013 in Yangtze River Delta region, China, *Sci*  
592 *Total Environ*, 603, 807-816, 2017.
- 593 Ren, Y., Qu, Z. L., Du, Y. Y., Xu, R. H., Ma, D. P., Yang, G. F., Shi, Y., Fan, X., Tani, A., Guo,  
594 P. P., Ge, Y., and Chang, J.: Air quality and health effects of biogenic volatile organic  
595 compounds emissions from urban green spaces and the mitigation strategies, *Environ Pollut*,  
596 230, 849-861, 2017.
- 597 Saha, S., Moorthi, S., Wu, X., Wang, J., Nadiga, S., Tripp, P., Behringer, D., Hou, Y.-T.,  
598 Chuang, H.-y., Iredell, M., Ek, M., Meng, J., Yang, R., Mendez, M. P., van den Dool, H., Zhang,  
599 Q., Wang, W., Chen, M., and Becker, E.: The NCEP Climate Forecast System version 2, *J*  
600 *Climat*, 27, 2185-2208, 10.1175/JCLI-D-12-00823.1, 2013.
- 601 Shao, M., Lu, S. H., Liu, Y., Xie, X., Chang, C. C., Huang, S., and Chen, Z. M.: Volatile organic  
602 compounds measured in summer in Beijing and their role in ground-level ozone formation, *J*  
603 *Geophys Res-Atmos*, 114, 2009.
- 604 Sillman, S.: The use of NO<sub>y</sub>, H<sub>2</sub>O<sub>2</sub>, and HNO<sub>3</sub> as indicators for ozone-NO<sub>x</sub>-hydrocarbon  
605 sensitivity in urban locations, *J Geophys Res-Atmos*, 100, 14175-14188, 1995.
- 606 Sillman, S.: The relation between ozone, NO<sub>x</sub> and hydrocarbons in urban and polluted rural  
607 environments, *Atmos Environ*, 33, 1821-1845, 1999.
- 608 Soriano, J. B., et al.: Global, regional, and national deaths, prevalence, disability-adjusted life  
609 years, and years lived with disability for chronic obstructive pulmonary disease and asthma,  
610 1990-2015: a systematic analysis for the Global Burden of Disease Study 2015, *Lancet Resp*  
611 *Med*, 5, 691-706, 10.1016/S2213-2600(17)30293-X, 2017.
- 612 Stavrakou, T., Muller, J. F., Bauwens, M., De Smedt, I., Van Roozendaal, M., Guenther, A.,  
613 Wild, M., and Xia, X.: Isoprene emissions over Asia 1979-2012: Impact of climate and land-use  
614 changes, *Atmos Chem Phys*, 14, 4587-4605, 10.5194/acp-14-4587-2014, 2014.
- 615 Sun, L., Xue, L., Wang, Y., Li, L., Lin, J., Ni, R., Yan, Y., Chen, L., Li, J., Zhang, Q., and Wang,  
616 W.: Impacts of meteorology and emissions on summertime surface ozone increases over central



- 617 eastern China between 2003 and 2015, *Atmos Chem Phys*, 19, 1455-1469, 10.5194/acp-19-1455-  
618 2019, 2019.
- 619 Sun, W. X., Hess, P., and Liu, C. J.: The impact of meteorological persistence on the distribution  
620 and extremes of ozone, *Geophys Res Lett*, 44, 1545-1553, 10.1002/2016gl071731, 2017.
- 621 Tonnesen, G. S., and Dennis, R. L.: Analysis of radical propagation efficiency to assess ozone  
622 sensitivity to hydrocarbons and NO<sub>x</sub> 1. Local indicators of instantaneous odd oxygen production  
623 sensitivity, *J Geophys Res-Atmos*, 105, 9213-9225, 2000.
- 624 Wang, J., Zhao, B., Wang, S., Yang, F., Jia, X., Morawska, L., Ding, A., Kulmala, M.,  
625 Kerminen, V. M., and Kujansuu, J. J. S. o. t. T. E.: Particulate matter pollution over China and  
626 the effects of control policies, 584-585, 426, 2017.
- 627 Wang, Q. G., Han, Z. W., Wang, T. J., and Zhang, R. J.: Impacts of biogenic emissions of VOC  
628 and NO<sub>x</sub> on tropospheric ozone during summertime in eastern China, *Sci Total Environ*, 395,  
629 41-49, 10.1016/j.scitotenv.2008.01.059, 2008.
- 630 Wang, S. X., Zhao, B., Cai, S. Y., Klimont, Z., Nielsen, C. P., Morikawa, T., Woo, J. H., Kim,  
631 Y., Fu, X., Xu, J. Y., Hao, J. M., and He, K. B.: Emission trends and mitigation options for air  
632 pollutants in East Asia, *Atmos Chem Phys*, 14, 6571-6603, DOI 10.5194/acp-14-6571-2014,  
633 2014.
- 634 Xing, J., Wang, S. X., Jang, C., Zhu, Y., and Hao, J. M.: Nonlinear response of ozone to  
635 precursor emission changes in China: A modeling study using response surface methodology,  
636 *Atmos Chem Phys*, 11, 5027-5044, 2011.
- 637 Yang, X., Xue, L. K., Wang, T., Wang, X. F., Gao, J., Lee, S. C., Blake, D. R., Chai, F. H., and  
638 Wang, W. X.: Observations and explicit modeling of summertime carbonyl formation in Beijing:  
639 Identification of key precursor species and their Impact on atmospheric oxidation chemistry, *J*  
640 *Geophys Res-Atmos*, 123, 1426-1440, 2018.
- 641 Zhang, G., Gao, Y., Cai, W., Leung, L. R., Wang, S., Zhao, B., Wang, M., Shan, H., Yao, X.,  
642 and Gao, H.: Seesaw haze pollution in North China modulated by the sub-seasonal variability of  
643 atmospheric circulation, *Atmos Chem Phys*, 19, 565-576, 10.5194/acp-19-565-2019, 2019.
- 644 Zhang, J. X., Gao, Y., Luo, K., Leung, L. R., Zhang, Y., Wang, K., and Fan, J. R.: Impacts of  
645 compound extreme weather events on ozone in the present and future, *Atmos Chem Phys*, 18,  
646 9861-9877, 10.5194/acp-18-9861-2018, 2018.
- 647 Zhang, Q., Yuan, B., Shao, M., Wang, X., Lu, S., Lu, K., Wang, M., Chen, L., Chang, C. C., and  
648 Liu, S. C.: Variations of ground-level O<sub>3</sub> and its precursors in Beijing in summertime between  
649 2005 and 2011, *Atmos Chem Phys*, 14, 6089-6101, 10.5194/acp-14-6089-2014, 2014.



- 650 Zhang, Y. Z., and Wang, Y. H.: Climate-driven ground-level ozone extreme in the fall over the  
651 Southeast United States, *Proc Natl Acad Sci USA*, 113, 10025-10030,  
652 10.1073/pnas.1602563113, 2016.
- 653 Zhao, B., Wang, S. X., Liu, H., Xu, J. Y., Fu, K., Klimont, Z., Hao, J. M., He, K. B., Cofala, J.,  
654 and Amann, M.: NO<sub>x</sub> emissions in China: Historical trends and future perspectives, *Atmos*  
655 *Chem Phys*, 13, 9869-9897, DOI 10.5194/acp-13-9869-2013, 2013.
- 656 Zhao, B., Wu, W. J., Wang, S. X., Xing, J., Chang, X., Liou, K. N., Jiang, J. H., Gu, Y., Jang, C.,  
657 Fu, J. S., Zhu, Y., Wang, J. D., Lin, Y., and Hao, J. M.: A modeling study of the nonlinear  
658 response of fine particles to air pollutant emissions in the Beijing-Tianjin-Hebei region, *Atmos*  
659 *Chem Phys*, 17, 12031-12050, DOI 10.5194/acp-17-12031-2017, 2017.
- 660 Zhao, B., Zheng, H. T., Wang, S. X., Smith, K. R., Lu, X., Aunan, K., Gu, Y., Wang, Y., Ding,  
661 D., Xing, J., Fu, X., Yang, X. D., Liou, K. N., and Hao, J. M.: Change in household fuels  
662 dominates the decrease in PM<sub>2.5</sub> exposure and premature mortality in China in 2005-2015, *Proc*  
663 *Natl Acad Sci USA*, 115, 12401-12406, 2018.
- 664 Zhao, S. P., Yu, Y., Yin, D. Y., He, J. J., Liu, N., Qu, J. J., and Xiao, J. H.: Annual and diurnal  
665 variations of gaseous and particulate pollutants in 31 provincial capital cities based on in situ air  
666 quality monitoring data from China National Environmental Monitoring Center, *Environ Int*, 86,  
667 92-106, 10.1016/j.envint.2015.11.003, 2016.
- 668 Zheng, B., Tong, D., Li, M., Liu, F., Hong, C. P., Geng, G. N., Li, H. Y., Li, X., Peng, L. Q., Qi,  
669 J., Yan, L., Zhang, Y. X., Zhao, H. Y., Zheng, Y. X., He, K. B., and Zhang, Q.: Trends in China's  
670 anthropogenic emissions since 2010 as the consequence of clean air actions, *Atmos Chem Phys*,  
671 18, 14095-14111, 2018.
- 672 Zheng, G. J., Duan, F. K., Su, H., Ma, Y. L., Cheng, Y., Zheng, B., Zhang, Q., Huang, T.,  
673 Kimoto, T., Chang, D., Poschl, U., Cheng, Y. F., and He, K. B.: Exploring the severe winter haze  
674 in Beijing: the impact of synoptic weather, regional transport and heterogeneous reactions,  
675 *Atmos Chem Phys*, 15, 2969-2983, 2015.
- 676